

Structural Development, Analysis, and Testing of a Full Scale Jet Vane Thrust Vector Control Rocket for Active Stabilization

Pritham Sathish*, Kush Bandi[†], Margaret Hwang[‡], Atharva Gujrathi[§], Anjali Yagnavajhala[¶], Alex Zangara^{||}, Michael Yore**, Shalini Shailesh^{††}, Christina Wang^{‡‡}, Taehan Lee^{§§}
Georgia Institute of Technology, Atlanta, GA, 30332

Jet vane thrust vector control (JVTVC) is a method of active stabilization by actuating control surfaces placed in the exhaust to manipulate the rocket's attitude. This paper describes the work of the Guidance, Navigation, and Control (GNC) team at Georgia Institute of Technology's Ramblin' Rocket Club in the development and analyses of the structural subsystems for an actively stabilized solid-propellant rocket using JVTVC. The development of this rocket was split up into four phases: design, analysis, manufacturing, and testing. During the design phase, the rocket was sectioned into an upper, transition, and lower section. Each subsystem was designed for manufacturability, structural integrity, modularity, and ease of integration. Various analysis techniques were used to ensure mission success, including FEA analysis on transition and jet vane assemblies, hand calculations for snatch loads acting on recovery bulkheads, and fin flutter analysis to characterize carbon-fiber layup requirements. During the testing phase, three static fires were completed to assess the feasibility of jet vanes, with a final static fire scheduled for a future test. Additionally, parachute deployment was tested to simulate recovery procedures, and jet vane control mechanisms were integrated with software to analyze control inputs during flight. The development of the JVTVC rocket showcases the complete engineering life cycle, from design and analysis to testing and iteration, resulting in a modular and reliable system for active stabilization. This project validates the feasibility of jet vane control and recovery procedures, contributing to advancements in thrust vector control technologies for amateur rocketry.

Nomenclature

a	=	Speed of sound
A	=	Fin aspect ratio
c	=	Chord
E	=	Elastic modulus
G	=	Shear modulus
G_E	=	Effective shear modulus
k_{sc}	=	Spring constant of shock cord
L_{sc}	=	Length of shock cord
m_{us}	=	Mass of Upper Section
p	=	Fluid pressure
p_0	=	Air pressure at sea level
t	=	Thickness
V_f	=	Flutter velocity

*Structures Co-Lead, GT Ramblin' Rocket Club, Aerospace Engineering, AIAA Undergraduate Student Member 1536656

[†]Structures Co-Lead, GT Ramblin' Rocket Club, Aerospace Engineering, AIAA Undergraduate Student Member 1603558

[‡]Systems Co-Lead, GT Ramblin' Rocket Club, Aerospace Engineering, AIAA Undergraduate Student Member 1603466

[§]Structures Co-Lead, GT Ramblin' Rocket Club, Aerospace Engineering, AIAA Undergraduate Student Member 1603265

[¶]Structures Member, GT Ramblin' Rocket Club, Aerospace Engineering, AIAA Undergraduate Student Member 1810166

^{||}Structures Member, GT Ramblin' Rocket Club, Aerospace Engineering, AIAA Undergraduate Student Member 1811146

**Structures Member, GT Ramblin' Rocket Club, Aerospace Engineering, AIAA Undergraduate Student Member 1811107

^{††}Structures Member, GT Ramblin' Rocket Club, Aerospace Engineering, AIAA Undergraduate Student Member 1603240

^{‡‡}Structures Member, GT Ramblin' Rocket Club, Aerospace Engineering, AIAA Undergraduate Student Member 1811062

^{§§}Structures Member, GT Ramblin' Rocket Club, Aerospace Engineering, AIAA Undergraduate Student Member 1742748

- V_{us} = Velocity of upper section after deployment
- x_{sc} = Stretch distance of shock cord
- λ = Taper ratio

I. Introduction

In Fall 2023, the Georgia Tech Guidance, Navigation, and Control (GT GNC) team began the mission to become the first collegiate team to build a thrust vector-controlled (TVC) rocket via jet vane control using solid rocket propulsion. The mission began with the desire to contribute knowledge to a critical area in rocketry: achieving rapid and agile controls to maintain flight along a desired trajectory while setting a precedent for collegiate teams. Development of the jet vanes rocket (JVR) began with the goal of conducting several static fires to validate the control mechanisms and authority. During the first year of development, GNC faced a steep learning curve throughout the testing and design process, but each lesson learned contributed towards the refinement of the mechanical design, hardware and software architecture, control algorithm, and integration processes. With each static fire, GNC has gained greater insight into what system requirements define a successful jet vane thrust vector control (JVTVC) system.

The JVR was developed through a four-stage process: design, analysis, manufacturing, and testing. The design phase involved iterative refinements and verification of system requirements, followed by analysis of critical subsystems to identify and address potential failure points. Manufacturing focused on producing components that met design specifications while ensuring ease of integration and assembly. Finally, the testing validated subsystem functionality, with improvements based on results. This structured approach optimized the JVTVC, aerodynamic stability, and structural integrity, addressing challenges such as vane erosion, thrust loss, and active stability control. This paper discusses the design and testing methodology of the current JVR, a culmination of two years of research and work by over 50 students.

II. Rocket Overview

The JVR architecture follows the extensively-tested standard rocket designs of high-powered-rocketry (HPR) and is comprised of two sections: an 8" diameter lower section and a 6" diameter upper section. The upper stage contains recovery hardware, comprised of the drogue and main parachutes, as well as two multipurpose avionics bays that house custom-built GNC avionics and custom off-the-shelf (COTS) avionics respectively. The lower stage contains the rocket motor, an AeroTech N1000W-PS COTS motor, which has a long burn time of 13.1 seconds. This is ideal for TVC where an increased burn time provides greater opportunity for controlled flight.

The high-level design and simulation of the rocket were created using OpenRocket and refined with the SOLIDWORKS CAD software. After multiple design phases, the final structural design was finalized, as seen in Fig. 1.

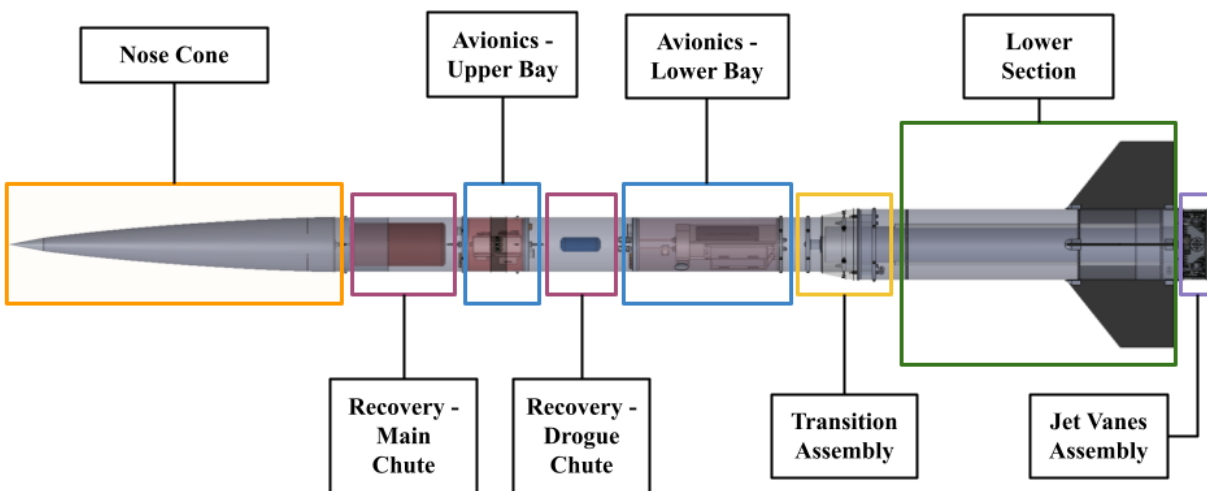


Fig. 1 Full rocket overview.

The following flight parameters were derived from the OpenRocket model and provided insight regarding rocket liftoff, ascent, and descent, which are critical to the vehicle design.

Table 1 Jet Vanes Rocket Performance Parameters

Parameter	Value	Parameter	Value
Apogee	9396 ft	Stability	1.88
T/W Liftoff (max)	5.5	T/W Liftoff (off rail)	2.6
Max Speed	M = 0.614	Max Acceleration	4.3 Gs
Wet Mass	90.7 lbs	Dry Mass	73.18 lbs

The rocket is designed with JVTVC to actively stabilize its orientation in the roll, pitch, and yaw axes. Approximately halfway through the burn time, the planned flight trajectory involves turning to and holding a 5° yaw adjustment. This further tests the JVTVC system’s capability to actively stabilize and react to aerodynamic loading.

III. Jet Vane Assembly

The development of the JVR began with the design of the jet vane assembly (JVA). Comprised of structural and drivetrain sub-assemblies, the JVA provides jet vane stability while enduring full burn of the N1000-W motor. The structural subassembly provides a robust interface between the jet vane drivetrain and rocket airframe while withstanding various thrust loading conditions. A “sandwich” mounting architecture is implemented, where a vertical plate carrying the cantilevered vane drivetrain is packed between two plates, shown in Fig. 2. This configuration ensures that the assembly retains a high strength-to-weight ratio and can be fabricated with simple 2D manufacturing operations.

The drivetrain subassembly facilitates the transfer of rotational actuator control to the jet vanes while operating under torque requirements provided by the simulations team. The selected positional-feedback servo motor ensures the drivetrain retains an ample torque factor of safety (FoS) of 7.6. The drivetrain employs a two-stage geared-down architecture that advantageously distances actuators from high-temperature flow regimes. Transfer of rotational power to the jet vanes is achieved by integrating COTS components in the custom-machined structural assembly. The jet vane was iteratively selected to be a high-purity tungsten and designed with minimal features to reduce complex manufacturing operations. In addition, a jet vane mount was developed to interface the vanes with the COTS drivetrain components which are composed of Ti-6Al-4V titanium alloy for its low thermal conductivity.

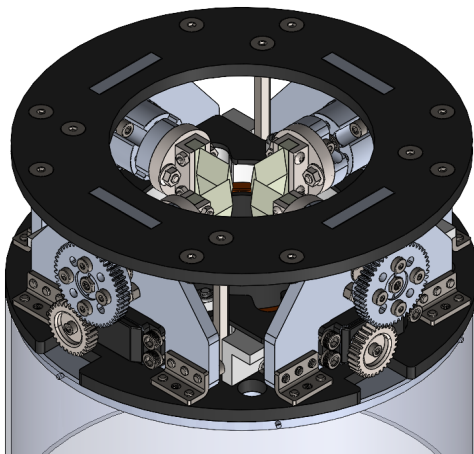


Fig. 2 3D model of the jet vanes assembly.



Fig. 3 Fully assembled jet vanes assembly.

Fig. 4 The jet vanes assembly of the jet vanes rocket.

IV. Lower Section

A. Fin Design

A trapezoidal fin geometry was chosen to provide the required stability margin of 1.5 calibers as verified by OpenRocket simulations. Another design consideration was the fin cant - the fin angle with respect to the rocket's vertical axis. For this application, minimizing the fin cant is important to prevent passive roll rate which decreases control authority of the rocket. The fins were aligned with the jet vanes to ensure the passively stabilizing forces from the fins align with actively stabilizing forces from the jet vanes.

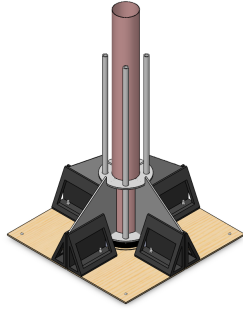


Fig. 5 The internal assembly shown on the fin jig.

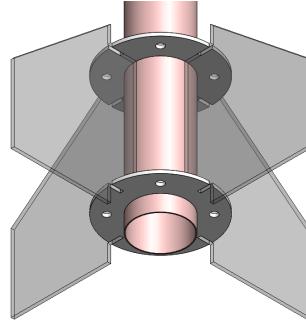


Fig. 6 The fins slot into the centering rings.

Figure 5 displays a fin jig designed to minimize the fin cant for this rocket. The jig supports the inner airframe and aligns the centering rings and fins to bond the components with epoxy in the correct orientations. Furthermore, the centering rings have cutouts that align with the fins, shown in Fig.6, which also ensures minimal cant. Fillets were applied between the fins and the body tube using Proline 4500 Epoxy to act as an aerodynamic and structural fairing.

B. Flutter Analysis

Flutter is an aeroelastic phenomenon caused by the elasticity of the lifting surface material and the aerodynamic loads it experiences. Together, these result in coupled bending-torsion oscillations. At a certain critical velocity, these oscillations become unsteady and diverge, potentially causing plastic deformation or fracturing of the fins. An important requirement of this rocket is that its maximum velocity retains a FoS of two with respect to critical flutter velocity; the flutter velocity is primarily a function of fin stiffness and shear modulus, which can be improved with laminating layups.

Carbon fiber layups are often used in HPR in order to improve the structural properties of the fin. Composite material analysis was performed to determine the minimum shear modulus required to prevent flutter. This determines whether layups are required and, if so, how many layers. The material for the fins is G10 core for added stiffness. Carbon fiber was used for the laminate material, and US Composites 635 3:1 epoxy hardener was used as the matrix. Table 2 contains the material properties of these components. Material properties were found from [1] [2] [3].

Table 2 Material Properties of Layup Components

	E (GPa)	Poisson's Ratio	G (GPa)
G10 Core	28.0	0.150	4.1
635 Epoxy	2.76	N/A	N/A
Carbon Fiber	231.7	N/A	N/A

Classical laminate theory [4] was used to approximate G_E of the laminate using the properties of each material component described in the table.

$$\left(\frac{V_f}{a}\right)^2 = \frac{G_E}{\frac{39.3A^3}{\left(\frac{t}{c}\right)^3(A+2)} \left(\frac{\lambda+1}{2}\right) \left(\frac{p}{P_0}\right)} \quad (1)$$

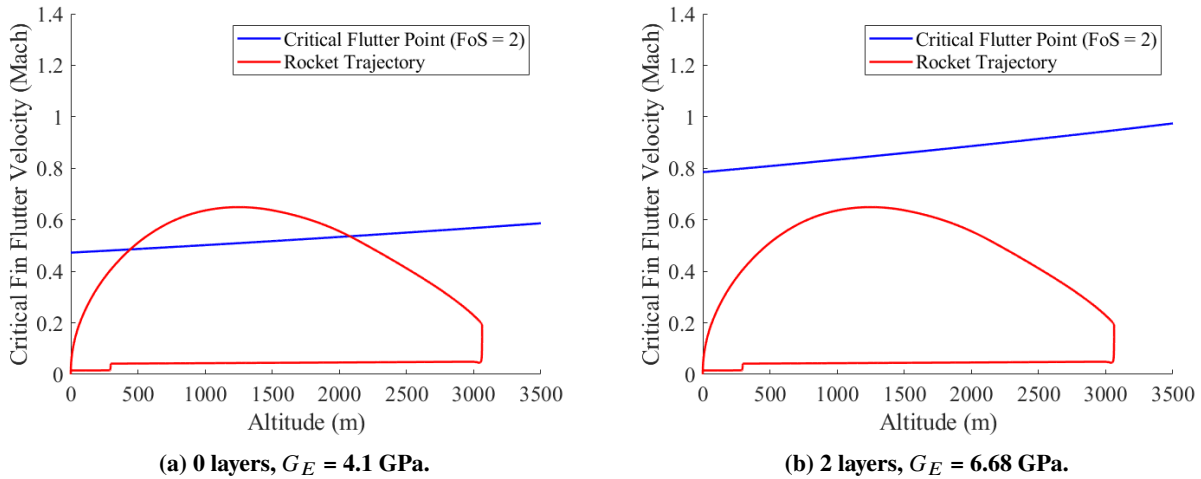


Fig. 7 The critical flutter point of the 2 layer composite exceeded the rocket's maximum velocity.

The critical flutter velocity, given by Eq. (1) referenced from [5], was found using the calculated G_E , and compared to the rocket's trajectory as seen in Fig. 7, imported from OpenRocket. G_E was first calculated for no layups, but based on the rocket's trajectory, fin flutter would occur. Then, two layers of bi-directional plies in a $[-45/45/0/90]_s$ orientation were added to achieve quasi-isotropic properties. One layer was not tested because this would result in orthotropic properties. G_E was then calculated for two layers of layups and then used to approximate critical flutter velocity, accounting for the increased thickness of the composite. This critical flutter velocity was then compared to the rocket's trajectory as seen in Fig. 7, and was determined to be higher than the rocket's maximum velocity. Thus, two layers of carbon fiber layups were determined sufficient to prevent fin flutter.

C. Layups

The fin layups use a "tip-to-tip" configuration. A single ply extends from the tip chord of one fin to the tip chord of another fin, as shown in Fig. 8. This provides additional torsional stiffness compared to a "sandwich" configuration, where layups are performed separately on each fin. The first ply of the carbon fiber layup is inset 0.75 inches from the second layer to prevent delamination. A layer of peel ply was placed over the layups to absorb excess epoxy and provide a rough finish for a good bonding surface. Before creating the rocket lay-ups, a practice lay-up was performed to ensure a valid procedure, shown in Fig. 9.

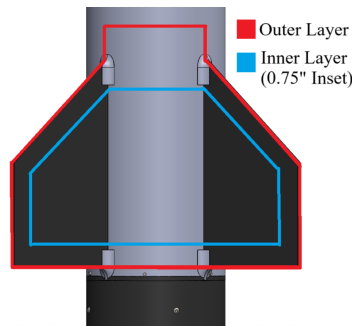


Fig. 8 The profiles for the carbon fiber layups are shown.

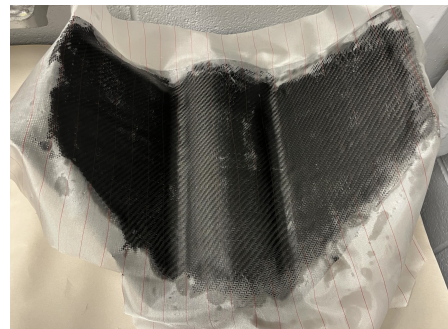


Fig. 9 The finished practice layup is shown on a lower section mock-up.

V. Transition Assembly

A. Transition Assembly Design

The transition assembly was designed to fulfill two main criteria: provide structurally stable internals to connect the lower section airframe and the upper section airframe and provide an aerodynamically shaped exterior to reduce drag.

The internal assembly was designed to withstand two main modes of failure – the bending moment about the center of the transition assembly and axial forces from drag during flight. The final design is comprised of three plates serving this dual purpose. Figure 10a. depicts the internal assembly. The “bottom plate” is fastened to the lower stage radially via radial screws and axially to the “middle plate” and “top plate” via standoffs. The middle plate sits flush on top of the lower stage and is fastened to the “aeroshell”. Lastly, the “top plate” is fastened radially to the upper stage. The three plates are made from aluminum, the fasteners are made from stainless steel, and the airframe tubes are G12 fiberglass.

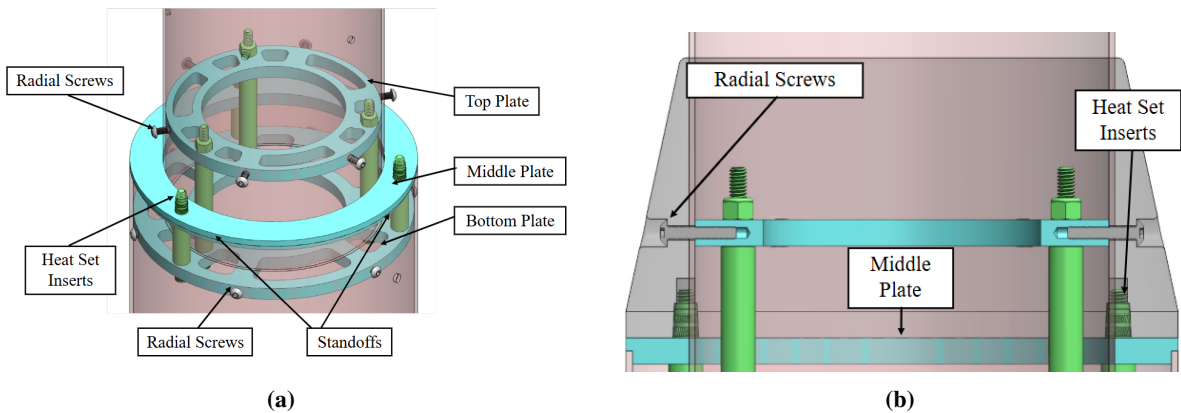


Fig. 10 Transition assembly internals and aeroshell.

The aeroshell is a 3D-printed cover that allows for airflow to curve around the 8-inch tube in a manner that minimizes drag and weight. It is made from Bambu Labs’ PA6-CF High-Temp Nylon Carbon Fiber material, selected for its high strength and thermal resistivity, along with its smooth surface finish, minimizing skin friction drag. This aeroshell is fastened to the middle plate via heat-set threaded inserts, also radially to the 6-inch tube and top plate. Figure 10b depicts the aeroshell fastening points.

B. Transition Assembly Validation

The main points of failure seen in rocket transition cones stem from bending failure. This occurs when the rocket incurs a non-zero angle of attack, and uneven drag forces create bending moments that concentrate around the radial fasteners [6]. Also, axial loads occur when the drag forces attempt to separate the two sections of the rocket.

To validate the strength of the fasteners along each point of contact, the aerodynamic forces acting on the rocket at a 10° angle of attack were computed using a computational fluid dynamics (CFD) aerodynamic model. Due to the limits of the control authority of the rocket, this was deemed to be the “worst-case-scenario” during flight. Ansys Mechanical was used to perform finite element analysis (FEA) on this system due to its availability and accuracy when calculating complex structural problems. Figure 11 depicts the applied force locations, with Table 3 denoting the load magnitudes. The forces involved the lift and drag forces on the fins, tubes, nose-cone, and transition aeroshell, along with a jet-vanes side force at its maximum deflection.

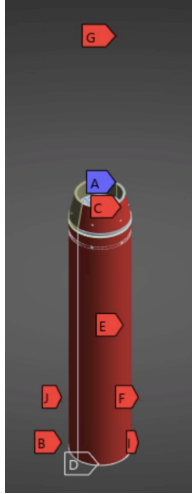


Fig. 11 Force locations in Ansys.

Table 3 Applied loads to respective force conditions

Boundary Condition Region	Boundary Condition Description	Applied Load (lbf)
A	Fixed Support	N/A
B	Fin 1 Force	219.18
C	Aeroshell Force	300.68
D	Jet Vanes Force	208.37
E	8-inch Airframe Force	169.51
F	Fin 2 Force	219.18
G	6-inch Airframe Force	31.368
H	Nosecone Force	444.72
I	Fin 3 Force	6.325
J	Fin 4 Force	6.325

The maximum stresses reported on each major sub-component are given in Table 4. A FoS is given based on the maximum tensile loads of each material.

Table 4 Maximum stress and factor of safety on transition assembly components.

Location	Maximum Stress (MPa)	Yield Strength (MPa)	Factor of Safety
Top Plate Radial Screws	71.224	482.63	6.8
Bottom Plate Radial Screws	160.94	482.63	3.0
Top Plate	33.258	241.00	7.2
Middle Plate	62.480	241.00	3.9
Bottom Plate	41.894	241.00	5.8
Aeroshell	6.3453	105 (100% infill)	16.5

VI. Upper Section

A. Recovery

The recovery system ensures the rocket returns to the ground safely using the deployment of a high-drag device. This rocket employs a dual-separation, dual-deployment system that ejects a drogue parachute at the apogee and a main parachute at 700 ft above ground, as represented in Fig. 12. The 2 ft diameter drogue parachute is located below the upper avionics bay, as seen in Fig. 1, and uses four ejection charges for complete redundancy - two from each avionics system. Under drogue chute deployment, the rocket will descend at 129 ft/s. The 10 ft. main parachute, presented in Fig. 1, is located below the nose cone and uses two ejection charges from the upper avionics bay. After main chute deployment, the rocket will slow to a descent of 19.6 ft/s. The delayed deployment of the main chute allows the rocket to land at a safe landing speed close to the launch site by decreasing the descent period.

Each of these recovery bays contains a shock cord attached from the top bulkhead U-bolts to the bottom bulkhead U-bolts, secured by a carabiner. Following standard HPR recovery practices, the length of each shock cord is determined by taking the length of the rocket and multiplying it by three, with the parachute attached to the top third of the cord. The ejection charges are initiated by E-matches, or detonator wires, which are connected to the avionics systems.

B. Upper Avionics Bay

The primary responsibility of the upper avionics bay is the deployment of the main parachute of the JVR with the additional capacity of supplying a redundant charge to the drogue parachute. It houses two altimeters, their respective

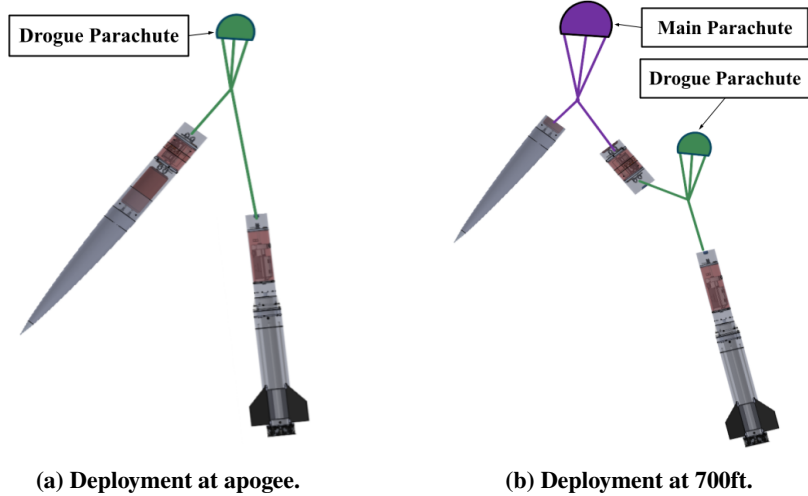


Fig. 12 Recovery stages in flight.

batteries, and screw switches for independent and external arming of components. At a pre-programmed altitude, one altimeter will send a high current signal to the charge-wells, igniting the pyrocharge, and deploying the main parachute. Additionally, the second altimeter functions to deploy the drogue parachute in the event an error occurs with the custom avionics pyrocharge. All components are mounted to a 3D-printed internal sled which is constrained to the bulkheads using threaded rods and lock-nuts. A fiberglass coupler tube protects the inner assembly, sandwiched between two aluminum bulkheads.

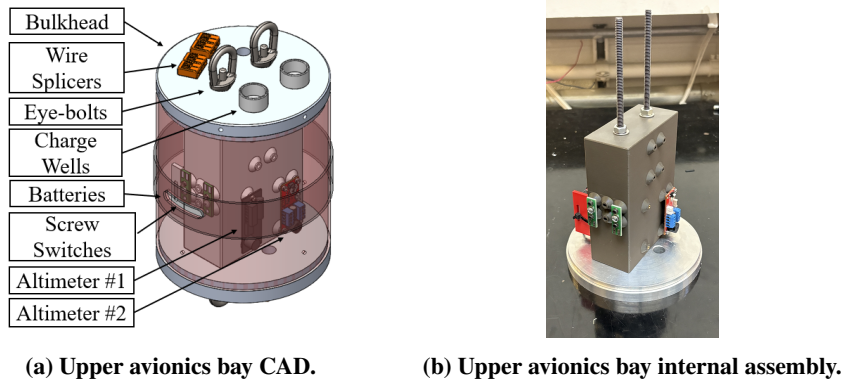


Fig. 13 Upper avionics bay pictures.

Additional analysis was performed to characterize the snatch forces on the top bulkhead of the upper avionics bay. A large velocity change occurs when the rocket is transitioning from the drogue to the main parachute, resulting in a short impulse of significant magnitude being sent through the shock cord and into the eyebolt. As a result, there is a possibility of shear failure of the eye-bolts from the threaded rods. To prevent this, the snatch force was calculated using the principle of conservation of energy. Total snatch force can be calculated as the sum of the kinetic energy of the vehicle and the elastic potential energy of the shock cord divided by the length of the cord used [7].

An estimated maximum force of 757.16 lbs was calculated; comparing this value to the yield strength for the steel eye-bolts results in a FoS of 1.3, ensuring that chances of shear failure occurring were improbable for this recovery system.

$$F = \frac{\frac{1}{2}m_{us}V_{us}^2 + \frac{1}{2}k_{sc}x_{sc}^2}{L_{sc}} \quad (2)$$

C. Lower Avionics Bay

The lower avionics bay contains the essential avionics and communications hardware for successful data acquisition, jet vanes control, and recovery system operations. The components housed within the bay are two custom boards, a GPS, and a radio antenna. The battery supplies power to our avionics systems, and its high voltage is managed by the PMS (Power Management System) board. Power from the PMS is routed to control and communications operations managed on the "Vaney" Flight Computer and to high current operations, including recovery charge deployment of the main parachute and servo actuation. An XT60 switch was integrated to allow for external arming of the recovery system. Similar to the upper avionics bay, components are mounted to a 3D-printed sled using threaded inserts and anchored onto threaded rods. The internal sled and rods are then constrained within a coupler tube and clamped together with two aluminum bulkheads and eye-bolts to complete the assembly.

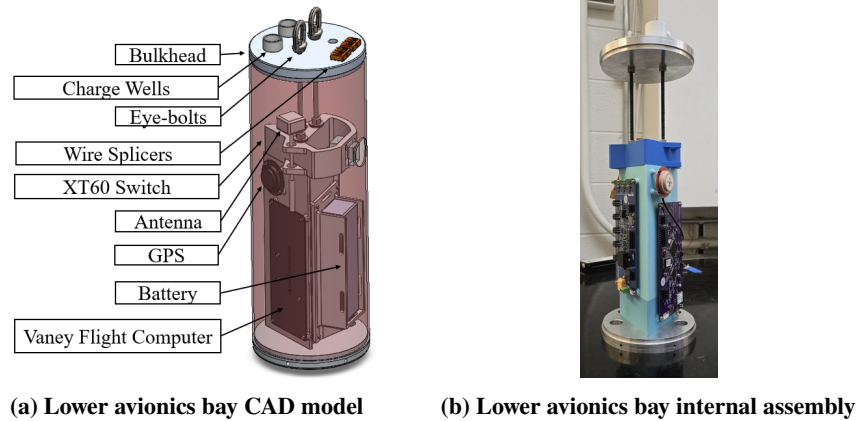


Fig. 14 Lower Avionics Bay Pictures

VII. Testing

A. Material Static Fire

The most critical design consideration for the jet vane assembly was the selection of vane material. A subscale static fire test stand was developed to experimentally validate four different materials (graphite, 4140 alloy steel, tungsten-copper, and tungsten-carbide) based on melting temperature, erosion resistance, and overall strength. Additionally, another goal of this static fire was to characterize the axial thrust loss experienced due to the vane geometry impeding the exhaust flow. Although the static fire proved successful, discrepancies between the motor used during this static fire (Cesaroni Technologies J293) and the intended motor to be used for the full JVR (AeroTech N1000W) prevented the results from being fully translatable. The post-fire examination showed that the tungsten-copper alloy experienced the least mass loss, making it the best candidate for future testing. To provide thorough validation and mimic flight conditions more accurately, a full-scale 98mm test stand was developed with additional goals of side force validation and axial thrust loss produced by the vane actuation.



Fig. 15 Material static fire test stand.

B. Pitch/Yaw Test Static Fire 1

The first static fire yielded inconclusive results as the components securing the vanes to the servos melted shortly after motor ignition, causing the vanes to detach entirely from the assembly. These results mainly provided motivation for the redesign of the jet vane assembly, resulting in the finalized configuration seen in Fig. 2.

C. Pitch/Yaw Test Static Fire 2

The second static fire aimed to demonstrate effective thrust vectoring from the jet vanes, proper side force characterization, and thrust loss; however, it fell short in these respects. Usable thrust loss and side force data could not be gathered because the jet vanes eroded shortly after the motor fired. The state of the jet vanes before and after the static fire can be seen in Figs. 16 and 17. Side force data was largely insignificant as most contact surfaces between jet vanes and the flow were eroded by the time rotation occurred. This data is shown in Fig. 18, and the side force expressed as a percentage of axial thrust is at most 1.2%. Similarly, accurate thrust loss due to the vanes impeding the flow couldn't be properly characterized. Brief thrust loss due to the vanes can be seen in Fig. 19, but this data cannot be extrapolated to the rest of the motor's burn time. However, a video recording of the static fire determined that the jet vanes actuators and structural assembly did function, as the jet vane backings rotated at the programmed rate and retained structural integrity. Excluding the vanes themselves, the structure of the jet vane assembly was overall successful. Although some unexpected flow recirculation onto the actuators and wires was observed, each component withstood the motor firing and was still functioning afterward.

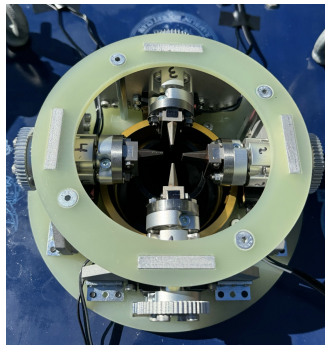


Fig. 16 Jet vanes before static fire.

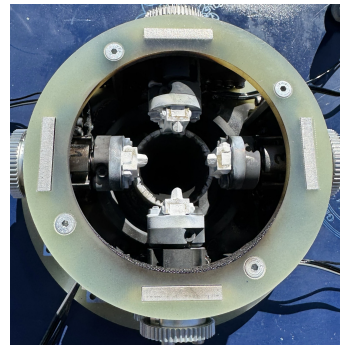


Fig. 17 Eroded jet vanes after static fire.

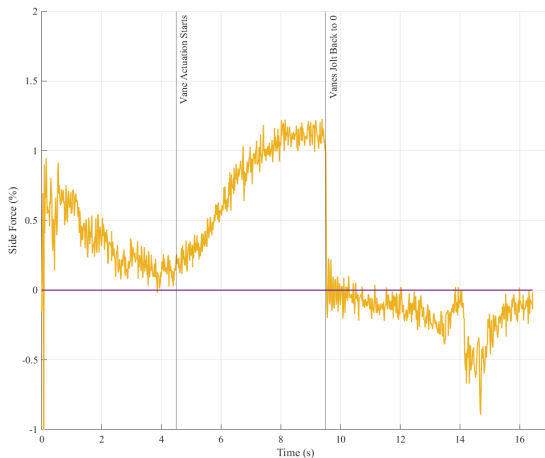


Fig. 18 Static fire 2 side force data.

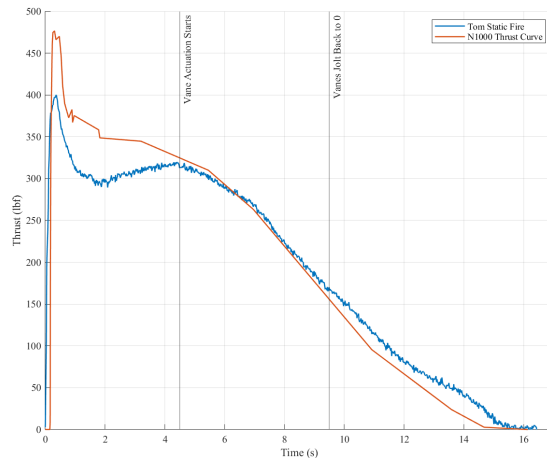


Fig. 19 Static fire 2 axial force data.

D. Pitch/Yaw Test Static Fire 3

The third static fire aims to improve on the shortcomings of the second static fire. The first and most crucial improvement was in the material selection of the jet vanes, which eroded during the second static fire when in contact with the motor's flow. Using the Mohs hardness scale, the only feasible option that will be able to withstand the motor's aluminum oxide particulate exhaust, which has an approximate Mohs hardness of 9, is pure tungsten, which also has a hardness of 9. Using tungsten vanes made manufacturing the primary constraint, so a new vane geometry was designed. Given that this component will be outsourced, the goal was to make the vane as simple as possible and so was modified

accordingly. Additionally, the servos controlling the jet vanes along with their wiring partially melted. To further protect these electrical components, an ablative thermal protection system was designed to shield the important drivetrain electrical components.

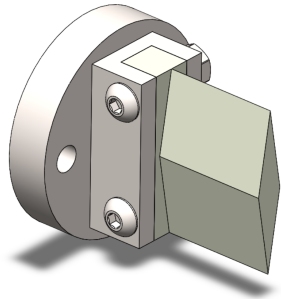


Fig. 20 New vane and vane backing geometry.

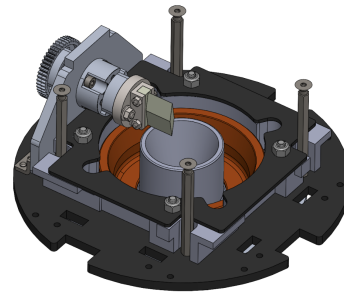


Fig. 21 Thermal protection system.

E. Deployment Testing

As previously discussed, the JVR utilizes a combination of a COTS parachute system and GNC's custom avionics system for the drogue chute. Deployment testing was conducted to determine the required amount of black powder for airframe separation during descent, ensuring successful parachute extraction. Additionally, these tests assessed the effectiveness of flame protection on the shock cords and parachutes. A preliminary mass of 1.5–2.5 grams of black powder was calculated using equations from [8] as an initial estimate for testing.

VIII. Conclusion

The JVR demonstrates the feasibility of the design, analysis, manufacturing, and testing of a jet vanes TVC rocket within a collegiate environment. By prioritizing design-for-manufacturing, modular subsystem architecture, and rigorous simulation and analysis, the process towards building the JVR sets a precedent for future collegiate rocketry initiatives. The iterative design approach involving design, simulation, and testing ensures a cost-effective process that can be scaled for larger missions while still providing a viable method of TVC for active stabilization in amateur rocketry. Until the launch of the JVR, GNC will continue to refine simulations and use the results of the launch to validate analysis methods. Ultimately, GTGNC aims to use results from the launch of the JVR to contribute to collegiate rocketry and the larger field of guided rocketry.

References

- [1] M.B. Kasen, D. B., G.R. MacDonald, and Schramm, R., "MECHANICAL, ELECTRICAL, AND THERMAL CHARACTERIZATION OF G-10CR AND G-11CR GLASS-CLOTH/EPOXY LAMINATES BETWEEN ROOM TEMPERATURE AND 4K," Tech. rep., National Bureau of Standards, Boulder, CO, 1980.
- [2] Fibreglast, "3K, 2 x 2 Twill Weave Carbon Fiber Datasheet," , 2025.
- [3] Composites, U., "635 EPOXY RESIN PRODUCT DATA," , 2013. <https://www.uscomposites.com/epoxy.html#epoxhard>.
- [4] Mallick, P., *FIBERREINFORCED COMPOSITES*, CRC Press, 2007.
- [5] Martin, D. J., "SUMMARY OF FLUTTER EXPERIENCES AS A GUIDE TO THE PRELIMINARY AS A GUIDE TO THE PRELIMINARY DESIGN OF LIFTING," Tech. rep., Langley Aeronautical Laboratory, Langley Field, VA, 1953.
- [6] Busse, J., and Kraft, G., *Aerobee 150 structural and aerodynamic pitch coupling*, National Aeronautics and Space Administration, 1966.
- [7] Newlands, R., "Parachute recovery system design for large rocket vehicles," Tech. rep., Aspire Space, UK, 2020.
- [8] NASA, "NASA Student Launch 2024: Advanced Rocketry Workshop – Recovery Systems," Tech. rep., 2023.